

Micro PIV analysis of secondary vortices with observations of primary vortices in single bubble cavitation microstreaming

J. Collis¹, A. Ooi¹ and R. Manasseh^{2,3}

¹Department of Mechanical Engineering
The University of Melbourne, Parkville, Victoria 3010, Australia

²Department of Mechanical Engineering
Swinburne University of Technology, Hawthorn, Victoria 3122, Australia

³Fluid Dynamics Group
CSIRO Materials Science & Engineering, Highett, Victoria 3190, Australia

Abstract

Cavitation microstreaming and Micro-PIV (Particle Image Velocimetry), the imaging techniques used to capture the flows, have gained increasing interest due to innovative medical treatments. Previous studies in microstreaming have focused entirely on the secondary flows, in the present study a novel technique has been used to capture the primary flow, within the Stokes layer, as well as studying significantly smaller bubbles. The speed of the flow within the Stokes layer is at least an order of magnitude larger than the secondary flows. Furthermore smaller bubbles tended to have shape irregularities which greatly affect the flow patterns produced.

Introduction

Cavitation microstreaming has gained increased interest in the past few years for innovative medical treatments such as sonoporation and sonothrombolysis [1, 2, 3, 4]; however, few flow visualizations or measurements of velocity fields and other significant metrics have been conducted. In this paper, work first conducted by Tho et al [2] has been further explored. Micro-PIV (Particle Image Velocimetry) measurements and streak photography were used to study the flow field around single 30-300 μm bubbles. The bubbles were held on the lower surface of a microchamber (pendant). Previous studies have focused on the visible secondary flow of cavitation microstreaming not the potentially more significant primary flow within the Stokes boundary layer. Since primary-flow velocities are much higher, they may exert stresses on nearby surfaces and be of much greater biological significance.

Micro-PIV system

The experimental apparatus has been developed from the equipment used by Tho *et al.* [2]. The significant change is the size and scale as well as the excitation parameters. The micro-PIV system consists of an inverted microscope, high-intensity light source, camera, acoustic excitation system and the microchamber. Figure 1 shows a diagrammatic view of the micro-PIV system. The microscope (Eclipse Ti-U, Nikon) has three objective lenses 4, 10 and 20 \times , the PIV pics were taken using the 20 \times lens. The lens has a narrow depth of field, 3.5 μm , allowing the formation of planes with a depth of 3.5 μm , however particles which are slightly out of focus produce larger, more dispersed but still coherent particles of light that are captured and contribute to the PIV analysis and hence giving planes a depth of $10 \pm 2 \mu\text{m}$.

Illumination source

The illumination source is a 100 W mercury arc lamp. The general optical path can be seen in Figure 1. As the light enters

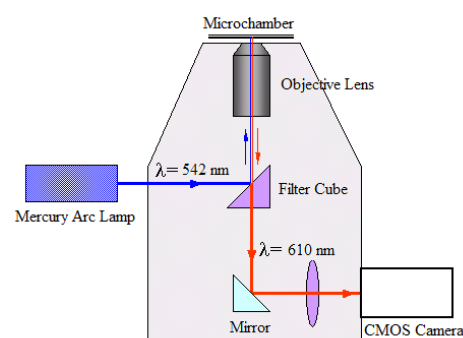


Figure 1: Diagrammatic experimental setup

the microscope it is directed to the filter cube. The filter cube (Chroma Technology Corp.) contains three filters, excitation, dichromatic beam splitter and emission filters. The light emitted from the mercury arc lamp contains a wide spread bandwidth of light, in order to remove as much pre-processing noise, light is filtered to only the desired wavelengths. Light first enters the excitation filter which removes everything except light in the bandwidth from 510 - 540 nm (green region). This light then passes straight into the second filter (dichromatic beam splitter/mirror) which functions both as a filter and a mirror. The dichromatic beam splitter acts as a high-pass filter with a transmission wavelength starting at 570 nm. Wavelengths below 570 nm are reflected up into and through the objective lens and onto the microchamber containing the solution of microspheres. The microspheres are coated in a red dye that is excited at a wavelength of 542 nm (green). On excitation, the dye fluoresces at a wavelength of 612 nm (red). The light emitted from the microspheres is collected by the objective lens and is directed back down towards the dichromatic beam splitter. Light that has passed back through the dichromatic beam splitter, light above 570 nm, then passes through the third and final emission filter. The emission filter has a narrow transmission bandwidth of 610 nm, this removes most of the background light (noise) whilst allowing the fluorescent light to pass through. After exiting the filter block the light is directed onto the camera's imaging chip. The camera is a high speed CMOS camera (Y3-Classic, Integrated Design Tools, Inc)

Acoustic excitation system

The acoustic source driving the microstreaming were one of either two ultrasound transducers (APC International Ltd.) which are of a sandwich construction. The frequency response of the transducers are non-linear and have a nominal resonant fre-

frequency of 28 and 40 kHz. The transducers were attached directly on the top surface of the microchamber and were connected via electrical leads to a single channel arbitrary function generator. The function generator (Tektronix AFG 3011) delivers a sinusoidal electrical waveform causing the ultrasound transducers to vibrate at the same frequency. The transducers were calibrated using a digital storage oscilloscope (Tektronix TDS 1012) and were found to have resonant frequencies of 28 ± 0.3 kHz and 40 ± 0.3 kHz respectively. These transducers were picked for their ability to provide excitation at or near the resonant frequency of bubbles smaller than that used by Tho *et al.* [2]. Using Minnaert's equation $f_M = \frac{1}{2\pi R_0} \sqrt{\frac{3\gamma p_0}{\rho}}$ as a guide we were able to determine a range of bubble sizes that would be able to be excited at or near the resonant frequency, 140-170 and 220-250 μm radius bubbles for the 40 and 28 kHz transducers respectively. The applied electrical waveforms are sinusoidal and were set to the resonant frequency of the individual transducers. The wavelength of sound through water can then be estimated to be between 51-55 mm and 36-38 mm. This is always greater than one order of magnitude larger than the depth of the microchamber (see below) and hence we can assume that the pressure wave within the chamber is spatially uniform. In these experiments the voltage amplitude of the sine wave was varied between peak to peak values of 3-20Vp-p.

Microchamber and preparation

The current experiments utilize two different microchambers (these chambers are termed microchambers for their sub-millimeter region of interest as opposed to chambers with sub-millimeter dimensions). The microchambers are thin rectangular cross sectional chambers which have the same cross-sectional area $35 \times 30 \text{ mm}^2$ and have depths of 1.5 mm and 3.5 mm. In addition the chambers have an 20 mm wall placed within the chamber to allow for additional points of view. The bottom and side walls are made from 1 mm clear perspex. The top of the chamber is made from 3 mm solid black perspex, to prevent any external light or reflections to enter the chamber and reduces the amount of noise within the chamber. The ultrasound transducer attach directly to the top of the microchamber. Figure 2 shows an example of the base of the microchamber with the reference coordinate system. As the microchamber can only be imaged from beneath due to the nature of the inverted microscope, the reference coordinate system is attached to the bubble with the X-Y plane being the plane parallel to the wall to which the bubble is attached, this will be discussed further in the next section. The microchamber is cleaned before each set of experiments with filtered water, sediment and chemical filters, and normal dishwashing soap to remove any particles and/or contaminants. The microchamber is then filled with room temperature (20-25 °C) filtered water and was seeded with 1 μm red fluorescent polymer microspheres (Fluoro-Max, Thermo Scientific), to a concentration of 0.0025 % vol/vol. The particles are excited by light at a wavelength of 542 nm (green) and once excited emit light at a wavelength of 612 nm (red). Once filled the microchamber is inspected and any air bubbles that are present are removed.

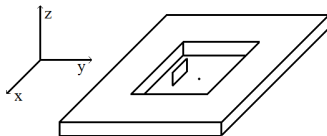


Figure 2: Microchamber base with reference coordinate system

Bubble preparation

Bubbles can be placed in the microchamber using two forms of attachment: pendant or captive. Pendant bubbles are bubbles which are held in place by surface tension forces alone whereas captive bubbles are held in place via surface tension and buoyancy forces. Pendant bubbles can be placed in one of two positions, either on the bottom of the microchamber or on the side of the inserted wall; captive bubbles are placed on the top of the chamber. Bubbles are delivered via a 0.5 μL syringe (SGE Analytical Science); bubble size is limited by the surface tension between the air, syringe needle and the water. Bubbles of 200-300 μm in diameter can be consistently produced. Each bubble is treated like a case study, a unique mode of microstreaming, as there are too many variables; size, shape, surface inhomogeneities and placement, which make it hard to replicate experimental conditions exactly.

Experimental Methods and Analysis

The PIV data is recorded using Motion Studio software (Integrated Design Tools, Inc); the frame rate of capture is 30 Hz and pictures are taken for one second for a total of thirty frames. The frames are split into fifteen sequential pairs of images using MATLAB (The Mathworks) and are saved as TIFF images. The images are processed using PIVview2C version 3.0 (PIVTEC GmbH), to obtain the velocity field for each pair of images. The raw PIV data is then processed using MATLAB to combine the data from the fifteen pairs of images and to remove any anomalies and outliers within the data set by using a form of low-pass filter on the magnitude as well as a directional filter.

Results and Discussion

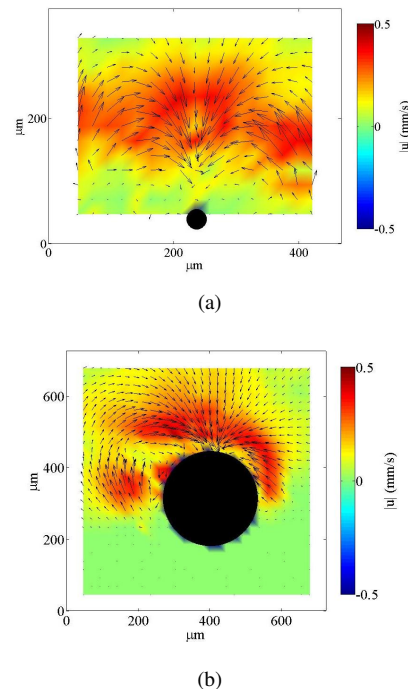


Figure 4: Two bubbles captured in the X-Z planes through the centre of the bubble; a) 30 μm diameter pendant bubble, centroid 20 μm from the bottom of the chamber, excited at 28 kHz 20 Vp-p, max velocity 0.54 mms^{-1} , max shear stress 0.0079 Pa, and b) 260 μm diameter pendant bubble, centroid 405 μm from the bottom of the chamber, excited at 28 kHz 16 Vp-p, max velocity 0.45 mms^{-1} , max shear stress 0.0071 Pa

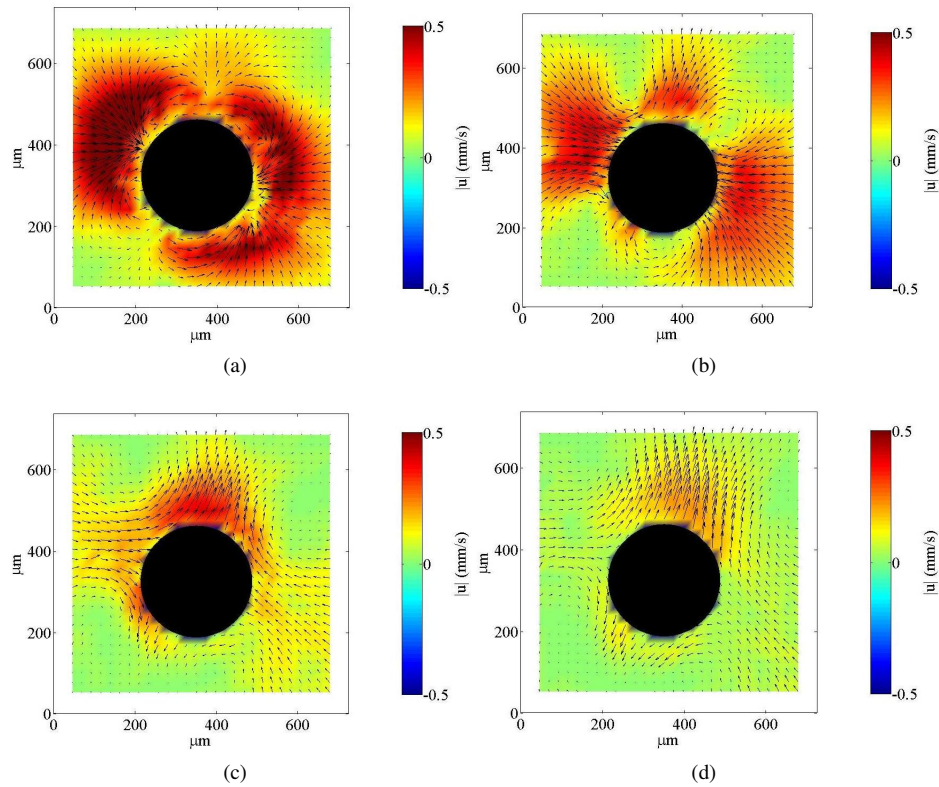


Figure 3: Four X-Y planes of a $250\ \mu\text{m}$ diameter pendant bubble excited at $28\ \text{kHz}$, $10\ \text{V}_p\text{-}p$, producing a quadrupole streaming pattern; a) $105\ \mu\text{m}$ from the wall plane, max velocity $0.68\ \text{mms}^{-1}$, max shear stress $0.0091\ \text{Pa}$, b) $180\ \mu\text{m}$ from the wall plane, max velocity $0.46\ \text{mms}^{-1}$, max shear stress $0.0055\ \text{Pa}$, c) $255\ \mu\text{m}$ from the wall plane, max velocity $0.41\ \text{mms}^{-1}$, max shear stress $0.0054\ \text{Pa}$ and d) $330\ \mu\text{m}$ from the wall plane, max velocity $0.22\ \text{mms}^{-1}$, max shear stress $0.0028\ \text{Pa}$

The results show similar patterns to those obtained by Tho *et al.* [2] as can be seen in Figure 3 and 4, as well as theoretical results on bubbles in the plane perpendicular to the wall as discussed by Lighthill and Riley [5, 6, 7] and experimental results by Marmottant and Hilgenfeldt [8]. The direction of the flows in Figure 4 appear to be in the opposite direction when compared to Lighthill, Riley and Marmottant and Hilgenfeldt [5, 6, 7, 8], although having the same pattern, suggesting that the mode of oscillation may differ slightly. This may be due to the bubble resting on a vertical wall and that the surface tension forces and buoyancy forces do not act along the same line of action, inducing a torsional element on the bubble. Gopinath [9] showed streamlines of similar pattern and direction produced by a sphere undergoing torsional oscillations in the vertical axis which may more accurately describe the oscillation of the bubbles in Figure 4. Throughout the current experiments, different patterns have been observed and whilst the frequency cannot be varied to obtain these different patterns, as shown by Collis *et al.* [1], the size of the bubble can be changed varying the frequency applied compared to the bubbles resonant frequency. Unfortunately the bubble oscillations are at too high of a frequency to capture the mode of oscillations. The exposure time required to obtain good PIV results in the current experiments is approximately $8000\ \mu\text{s}$ whilst the period of the oscillation is $35\ \mu\text{s}$ meaning that it is impossible to capture the bubble at different intervals of its oscillation, even with a triggered circuit. Although many oscillation modes and the resultant flow patterns have been well documented these modes of oscillation are of the most simplest forms, linear, 1-dimensional oscillations. Figure 5a shows the more commonly studied quadrupole pattern as shown by Tho *et al.* [2], albeit slightly skewed, de-

veloped by linear 1-dimensional oscillation along the boundary wall. However Figure 5b shows an unfamiliar pattern in which a single vortex is on one side of the bubble. This is extremely rare as flow patterns were generally found to be symmetrical. This single vortex maybe due to an irregularity in the shape of the bubble, caused by radial pressure being unable to overcome surface tension forces at the boundary of the bubble, and/or due to condensation droplets being formed within the bubble. These two phenomena observed were especially evident with bubbles less than $250\ \mu\text{m}$ in diameter. Kotas *et al.* [10] showed that the formation of a fifth vortex as well as the flow being highly skewed when an obliquely oscillated sphere with an aspect ratio of 0.5 was linearly translated, the typical pattern for this mode of oscillation would be a symmetrical quadrupole pattern. Although the oscillation was linear the pattern developed was quite irregular due to the oscillation not being in line with the axis of symmetry, the irregular shapes of the bubble in these experiments could be the cause of the flow pattern observed in Figure 5b. Although the voltage delivered to the transducer was less than or equal to that delivered to the piezoelectric disk used in Tho *et al.* [2] the maximum magnitude of the some of the key metrics of interest in the application of microbubbles, discussed by Collis *et al.* [1], were actually less than those obtained in the current experiments. This may be due to greater pressure fluctuations being developed by the transducer or from one or more of the variations of the experimental parameters: bubble size, frequency, size of seed particles. In Figure 6, fast moving particles can be seen at the gas-liquid interface of the bubble; these particles were observed to be moving at significantly faster rates than the secondary flows adjacent. These particles are close to being within the theoretical Stokes boundary layer;

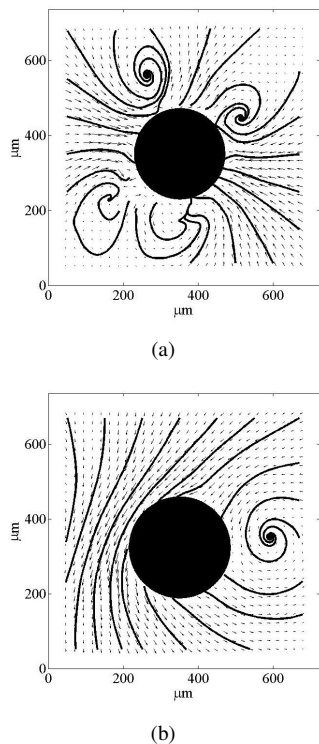


Figure 5: Two bubbles captured in the X-Y planes; a) 250 μm diameter pendant bubble excited at 28 kHz 10 Vp-p, max velocity 0.46 mms^{-1} , max shear stress 0.0055 Pa and b) 270 μm diameter pendant bubble excited at 28 kHz 10 Vp-p, max velocity 0.52 mms^{-1} , max shear stress 0.0059 Pa

furthermore they satisfy the flow criteria of the Stokes boundary layer: flow is parallel to the oscillating wall. The Stokes boundary layer is defined as $\delta = \sqrt{2\nu/\Omega}$, for the system under 28 kHz excitation is given to be approximately $3.5 \mu\text{m}$. The flow captured by these particles were also seen to be driving the clearly-visible secondary flows. The difficulty with capturing PIV data in small bubbles which are excited by high-frequency acoustics is that the Stokes layer is very small. As aforementioned the Stokes layer for the current setup is approximately $3.5 \mu\text{m}$, using $1 \mu\text{m}$ seeding particles its is possible to get seed particles into the Stokes layer. As the Stokes layer is extremely small there are not enough particles to perform PIV. However a novel technique using streak photography and varying the exposure time was used to approximate the speed of the flows within the Stokes layer. This is possible as the region of interest is very small and with a single particle present it is possible to track the entire path of the particle using streak photography. The exposure time was increased till the start and end of the path of the particle just touched. The speed of the flow within the top vortex was determined to be $13.35 \pm 2 \text{ mms}^{-1}$ which is twice an order of magnitude larger than the fastest secondary flow obtained in the experiments. The primary vortex speed calculation may not reflect the true velocity within the primary vortex as the particles within the layer may have affected the flow. As the Stokes layer is only $3.5 \mu\text{m}$, a $1 \mu\text{m}$ particle is nearly one third the size of the layer. This is significant and cannot be ignored, even though the density of the particles are closely matched to water.

Conclusion

A novel technique has been developed to measure the speed of primary flows, flows within the Stokes layer, developed by

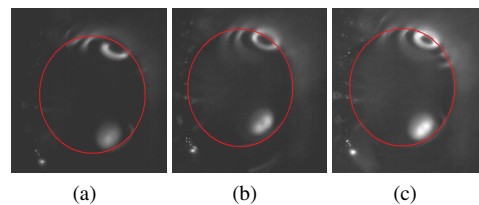


Figure 6: A 270 μm bubble excited at 28 kHz 20 Vp-p and captured in the X-Z plane with varying exposure to estimate the velocity of primary vortices at a speed of $13.35 \pm 2 \text{ mms}^{-1}$ a) exposure time of 5884 μs , b) exposure time of 8322 μs c) exposure time of 11767 μs

excited microbubble oscillations. The speed of the flow within the Stokes layer is at least an order of magnitude larger than the secondary flows. Subtle shape irregularities of the bubble may have a significant affect on the patterns produced especially if these irregularities are not along the same axis as the axis of oscillation. The modes of oscillation are not only sensitive to a change frequency but other parameters; size and shape of the bubble. When compared to the bubbles studies in Collis *et al.*, the present, smaller, bubbles tended to have larger maximum velocity and shear stress but steeper velocity gradients.

References

- [1] J. Collis, R. Manasseh, P. Liovic, P. Tho, A. Ooi, K. Petkovic-Duran and Y. Zhu, Cavitation microstreaming and stress fields created by microbubbles, *Ultrasonics*, 2010, 50, 273-279.
- [2] P. Tho, R. Manasseh and A. Ooi, Cavitation microstreaming patterns in single and multiple bubble systems, *J. Fluid Mech.*, 2007, 576, 191-233.
- [3] J. Wu, J. P. Ross and J. F. Chiu, Reparable sonoporation generated by microstreaming, *J. Acoust. Soc. Am.*, 2002, 111, 1460-1464.
- [4] N. McDannold, N. Vykhodtseva and K. Hynynen, Targeted disruption of the blood-brain barrier with focused ultrasound: association with cavitation activity, *Phys. Med. Biol.*, 2006, 51, 793-807.
- [5] Sir J. Lighthill, Acoustic streaming, *Journal of Sound and Vibration*, 1978, 61, 391-418.
- [6] N. Riley, Steady streaming, *Annu. Rev. Fluid Mech.*, 2001, 33, 43-65.
- [7] N. Riley, On a sphere oscillating in a viscous fluid, *Quart. Journ. Mech. and Applied Math.*, 1966, XIX, 461-472.
- [8] P. Marmottant and S. Hilgenfeldt, An bubble-driven microfluidic transport element for bioengineering, *PNAS*, 2004, 101, 9523-9527.
- [9] A. Gopinath, Steady streaming due to small amplitude torsional oscillations of a sphere in a viscous fluid, *Quart. Journ. Mech. and Applied Math.*, 1993, 46, 501-520.
- [10] C. W. Kotas, M. Yoda and P. H. Rogers, Visualization of steady streaming near oscillating spheroids, *Exp Fluids*, 2007, 43, 111-121.